Editors' Suggestion Featured in Physics

Structural Transformation between a Nematic Loose Packing and a Randomly Stacked Close Packing of Granular Disks

Yunhao Ding, Jing Yang, Chenyang Wang, Zhichao Wang, Jianqi Li, Bingwen Hu, and Chengjie Xia*
Shanghai Key Laboratory of Magnetic Resonance, School of Physics and Electronic Science, East China Normal University, Shanghai 200241, China

(Received 24 September 2022; accepted 29 June 2023; published 1 September 2023)

Packing structures of granular disks are reconstructed using magnetic resonance imaging techniques. As packing fraction increases, the packing structure transforms from a nematic loose packing to a dense packing with randomly oriented stacks. According to our model based on Edwards' volume ensemble, stack structures are statistically favored when the effective temperature decreases, which has a lower structural anisotropy than single disks, and brings down the global orientational order consequently. This mechanism identified in athermal granular materials can help us understand the nonergodic characteristics of disklike particle assemblies such as discotic mesogens and clays.

DOI: 10.1103/PhysRevLett.131.098202

Assemblies of disklike particles have aroused enduring research interests for more than half a century, and have many important technological applications [1], particularly due to their abilities in exhibiting abundant phases [2,3]. It is of both fundamental and practical importance in characterizing disks' packing configurations and predicting the phase behaviors using statistical mechanical tools [4–7]. Previous theoretical and numerical works have quantified thoroughly the thermal equilibrium isotropic, nematic, columnar, and cubatic phases of various disklike particles [8–12]. However, the actual phase behaviors in many experimental systems may go beyond the scope of these equilibrium-state researches, due to the existence of complex out-of-equilibrium characteristics, such as frustration between metastable states and a glasslike slowdown [13–15]. In particular, for disk systems with relatively large particle sizes, such as some clay materials, their phase behaviors could be dominated by the intrinsic athermal nature [16–19]. Hence, the statistical mechanism of these commonly studied materials in various related fields remains poorly understood. Moreover, previous experimental investigations have heavily relied on macroscopic measuring techniques to obtain globally averaged quantities [13,19,20], so that structural quantifications of disklike particle assemblies at particle level is missing, which prohibits microstructure-based understandings for their important transport and mechanical properties [21–23].

An alternative approach to study disklike particle assemblies is to use granular disks as a macroscopic model system. Direct observations of particle-scale structures of granular materials enable an analogous understanding of the phase behaviors and dynamics of their microscopic counterparts [24,25]. Also, a generalized equilibrium-state statistical mechanical framework of granular packings, i.e., the volume ensemble theory, has been established by Sir Edwards and co-workers [26], which assumes a Boltzmann-like sampling of all mechanically stable states with an effective temperature, also known as the compactivity. This framework has been used to derive jamming phase diagrams of spherical and nonspherical granular particles [27–29], and to understand the unique phase transformation mechanisms of granular materials [30–32]. Furthermore, a deep connection between granular packing and nonequilibrium glassy materials has been recognized [33–35]. For instance, a granular packing can be jammed in various mechanically stable states when external agitation ceases, which is analogous to a rapid quenching of a liquid state to its metastable inherent state in the (free-)energy landscape [36]. Therefore, a granular disk packing system can serve as a limiting nonequilibrium case as opposed to the thermal equilibrium systems studied previously. Investigating their phase behaviors based on a generalized statistical mechanical framework may provide a fundamental understanding to the commonly observed nonequilibrium characteristics of clay particles and discotic nematic liquid crystals. So far, studies of granular disks are extremely rare compared with those of other shapes [37], and even the geometric characteristics of their packing structures are yet to be revealed.

In this Letter, we report the results of a magnetic resonance imaging (MRI) study on a model granular disk system. We observe a curious structural transformation between a loose packing with a strong nematic order and a dense packing composed of short stacks with random orientations. Additionally, we reveal unusual structural features of the disk packings associated with stacks, including an incomplete local jamming condition, and a universal rescaled probability distribution of local packing volume for disks in different parts of a stack. Based on these experimental observations, we establish a mean-field

 © 2023 American Physical Society

model under the Edwards volume ensemble to explain the stack formation, and attribute the orientational disordering during compaction to a decreased anisotropy of excluded volume effect due to stack formation.

The granular disks used in this work are hollow plastic cylinders with a diameter $D = 30.75 \pm 0.07$ mm and thickness $H = 4.81 \pm 0.04$ mm. The packings were prepared in a $270 \times 206 \times 170$ mm^3 rectangular container, the internal walls of which are decorated with hemispheres with diameter 27 mm at random positions to diminish boundary-induced ordering effects. We adopt a packing compaction protocol inspired by an epitaxial growth. All disks were first divided into 1, 2, 5, or 10 batches and then poured randomly into the container in one batch after another, as the initial state of the compaction. The container was tapped for 30 times after each batch of disks was poured. Each tapping was conducted by dropping the container to the ground from a 1 cm height, and the container's base is parallel with the ground before dropping. This dropping height corresponds to a mild tapping intensity, with which we obtain the densest random packing state with a total of 300 taps (see the Supplemental Material [38] for details). Packings with different packing fractions are prepared with different batch numbers. Loose packings prepared by random pouring without tapping are also included. Each packing consists of 1200 disks, and approximately 500 disks whose centroids are at least $1D$ away from the container boundary are analyzed.

An MRI scanner (MAGNETOM Prisma Fit, Siemens Healthcare, Erlangen, Germany) was used to acquire the three-dimensional images of the packing. The granular disks are filled with hydrogels, which provide strong magnetic resonance signals, so that the images of individual disks appear separated even when they are in close contact. This allows a straightforward calculation of disk centroids and orientations (i.e., the normal direction of the disk face) with image processing, and a reconstruction of the packing structures [Figs. 1(b) and 1(c)], based on which various structural quantities can be evaluated. In particular, a

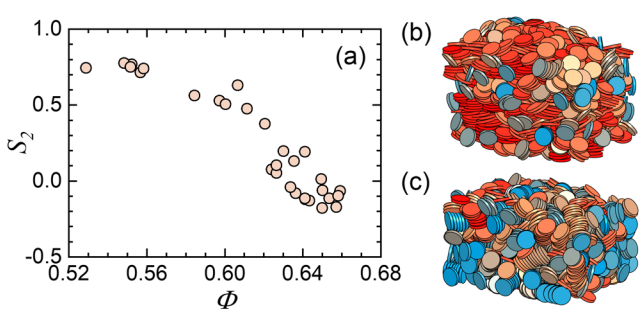

FIG. 1. (a) The nematic order parameters for packings with different Φ. (b),(c) Reconstructed packing structures with (b) $\Phi = 0.53$ and (c) 0.66. The disk color represents the angle between a disk's orientation and the vertical direction.

Voronoi tessellation of the packing structure is computed with a set-Voronoi algorithm [39]. Contacts between disks are identified with a generalized error-function-fitting method [40], by first calculating the shortest distances between a pair of disk's face, edge, or wall. There can be six different types of contacts between two disks: edge-edge (ee), edge-face (ef), edge-wall (ew), face-wall (fw), face-face (ff), and wall-wall (ww) contacts. Face-face (face-wall) contacts are identified with an additional criterion that the relative orientation of two disks should be smaller than 5° (larger than 85°). The detailed image-processing and contact identification methods are presented in the Supplemental Material [38]. In this work, the particle diameter D is set as the unit of length, and $V_d = 0.12$ is the volume of a single disk. The friction coefficient between disks is 0.63 ± 0.05, obtained by measuring the tangent of the maximal slope angle that stacked disks can maintain static with no sliding.

A first unexpected feature of our granular disk packings is the decreasing nematic order parameter $S_2 = \langle P_2(\cos\theta)\rangle$ with increasing packing fraction Φ [Fig. 1(a)]. P_2 is the second-order Legendre polynomial and θ is the angle between disk orientation and the director of the nematic phase (i.e., the gravitational direction). At first sight, it seems to be in contradiction with the Onsager's entropy-driven phase transition picture [41]. However, instead of a global order, stack structures composing face-contacting disks emerge as a typical local order, and the average stack size $\langle N_s\rangle$ (i.e., number of disks in a stack) increases with Φ [Fig. 2(b)]. Increasing local positional and orientational correlations due to stacks can also be clearly manifested through some conventional correlation functions, as presented in the Supplemental Material [38]. Two boundary states of a granular disk packing can be identified accordingly: a nematic loose packing and a randomly stacked dense packing. Hereafter, we explain this unusual structural transformation between the two states based on detailed characterizations of the packing structures.

The stack structures introduce an additional mesoscale feature into the system, making disks in the same packing statistically unequal. A disk may play three different roles in a packing: isolated disks with no ff contacts, which are defined as stacks with $N_s = 1$ (i.e., type 0), disks at either end of a stack (i.e., type 1), and disks inside a stack with ff contacts on both of its faces (i.e., type 2), and the local packing configuration of a disk depends strongly on its role in a stack (i.e., the type number) as demonstrated in the following. Thus, the packing structures are highly heterogeneous on the mesoscale of stacks. On the other hand, the large-range packing structures are rather uniform (see the correlation functions in the Supplemental Material [38]), which is probably due to the uncorrelated formation of stacks, as demonstrated in the exponential distributions of stack sizes N_s [Fig. 2(a)]. This also implies that the probability f of a disk joining a stack

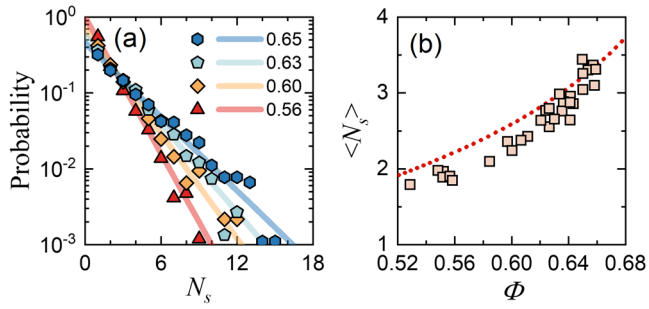

FIG. 2. (a) Probability distributions of stack size N_s for packings with different Φ: 0.65 (hexagons), 0.63 (pentagons), 0.60 (diamonds), and 0.56 (triangles). The solid lines are exponential fits. (b) Average stack size for packings with different Φ. The dotted line is the theoretical ensemble-averaging result.

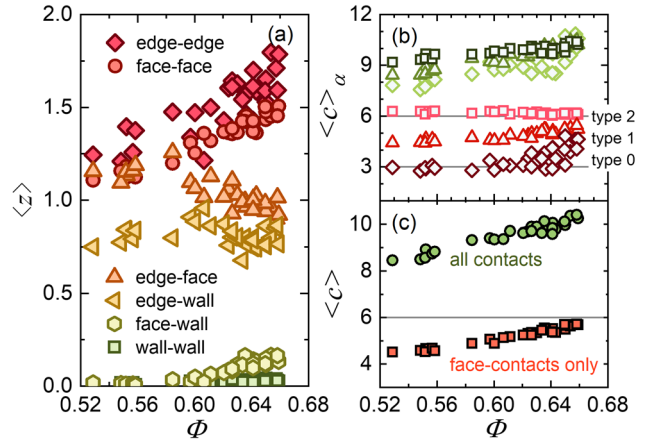

FIG. 3. (a) Average numbers of different forms of contacts $\langle z \rangle$ for packings with different Φ. (b) Averaged constraint number of type-α disks in each packing: $\langle c \rangle_\alpha$, where the average is taken over disks of type 0 (diamonds), 1 (triangles), and 2 (squares), respectively. (c) Averaged constraint number $\langle c \rangle$ of all disks in each packing. In panels (b) and (c), green symbols represent the average constraint numbers of all contacts, and red symbols represents those only counting contacts on disk faces. The solid lines in (b) represent the typical constraint numbers C_0 and C_2, and the one in (c) marks a generalized isostatic condition $\langle c \rangle = 6$.

is independent of N_s. Accordingly, the probabilities of finding a disk of the three types are $(1-f)^2$, $2f(1-f)$, and f^2, respectively. Therefore, f can be considered as a key state variable linking global packing properties with the representative particle-scale packing structures, through a probability-weighted averaging of the three types of disks.

We start characterizing particle-scale packing structures with contacts, which are crucial for understanding the jamming properties of a granular packing. An intriguing observation is that most disks can translate along directions perpendicular to their face normal vectors without causing overlaps with others (see the Supplemental Material [38] for details). This means that the geometric constraints of contacts on individual disks are incomplete, and only three degrees of freedom (d.o.f.) per disk (i.e., a translational and two orientational ones) on average are constrained by the contacts. The contact-type-dependent constraint numbers for frictionless particles are used: 1 for an ee, ef, ew, and ww contact, 2 for a wf contact, and 3 for an ff contact [42]. As shown in Fig. 3, the average constraint number C of all disks [Fig. 3(c)] and that of disks of any given type [Fig. 3(b)] increases with Φ, if all contacts between disks are included. Detailed analyses reveal that constraint number increases majorly due to ee and ff contacts, while numbers of other forms barely change with Φ [Fig. 3(a)]. More interestingly, if only contacts on the faces of each disk are included, the average constraint numbers of any types of disks are roughly constant [Fig. 3(c)]. Thus, to a first approximation, the increasing C with Φ is simply due to the increasing probability of disks to participate in stack structures. Furthermore, the average constraint number (that only includes contacts on faces) increases with Φ and approaches 6, which is just twice the number of actually constrained d.o.f. per disk, satisfying a generalized isostatic condition self-consistently. This $C(\Phi)$ equation of state crosses the boundary line separating random and ordered packings in the jamming phase diagram of spherelike particles [28,29], raising open questions on how to establish a correct phase diagram for granular packings having prominent ordering transformation when Φ changes.

We then examine packing volume fluctuation, which lies at the heart of the effective thermodynamics of granular packings. In contrast to granular sphere packings [40,43], the probability distribution functions (PDFs) of Voronoi cell volume $V_{\rm cell}$ show rather complex features like shoulders and double peaks, apparently resulting from the contributions of disks with different roles in stacks, whose separated PDFs are unimodal [Fig. 4(a)]. In addition, the separated PDFs of $V_{\rm cell}$ for disks with given types can be collapsed onto a master function when normalized by the average value, regardless of Φ and disk type [Fig. 4(b)]. Their identical relative fluctuations of $V_{\rm cell}$ imply an effective equilibration of the system. This leads to a proportional relation between the variance of $V_{\rm cell}$ and its square: $\mathrm{var}(V_{\rm cell}) = \sigma^2 \langle V_{\rm cell} \rangle^2$ for all three types of disks, where the dimensionless constant $\sigma^2 = 0.011$ is the variance of the master PDF. This universal relation can be generalized to an approximate equation relating the variance and average value of global packing volume $V_{\rm pack}$: $\mathrm{var}(V_{\rm pack}) \approx \sigma^2 \langle V_{\rm pack} \rangle^2 / N$, where N is the particle number (see the Supplemental Material for the derivation [40]). The compactivity χ (i.e., an effective temperature) of the packings can be calculated using this relation and an analogous thermodynamic fluctuation theorem: $\mathrm{var}(V_{\rm pack}) = \chi^2 \partial \langle V_{\rm pack} \rangle / \partial \chi$, under the Edwards framework [43,44]. We obtain $\chi = V_d \sigma^2 / (\Phi - \Phi_{\rm RLP})$ [Fig. 4(c)]. Here, the random loose packing (RLP) state is defined to have an infinite compactivity, and its packing

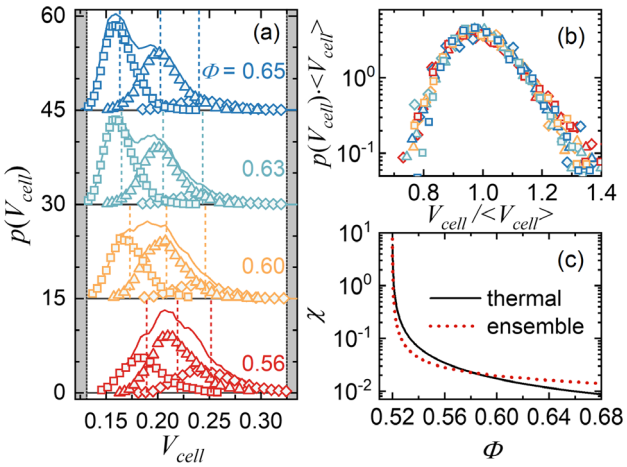

FIG. 4. (a) PDFs of Voronoi cell volume $V_{\rm cell}$ for packings with different Φ. The solid lines present PDFs of all disks' $V_{\rm cell}$, and the symbols represent separated PDFs of disks of type 0 (diamonds), 1 (triangles), and 2 (squares). The vertical dashed lines represent mean values of the separated PDFs. The gray regions' dotted borders mark the smallest and largest values of $V_{\rm cell}$: $V_d/0.92$ and $V_d/0.37$. (b) The PDFs of $V_{\rm cell}$ normalized by their averaged values. (c) The equation of state of compactivity versus packing fraction obtained by a thermodynamic integration of packing volume fluctuation (solid line) and ensemble averaging (dotted line).

fraction is set as $\Phi_{\rm RLP} = 0.52$, which is slightly smaller than that of our loosest packing. The Boltzmann constant is set as one.

The above results allow us to establish a minimal model for volume function (i.e., the Hamiltonian, which is the average free volume per particle), to calculate global structural quantities using the Edwards volume ensemble. As a mean-field model, we simplify the whole packing into a quasiparticle which is a superposition of the three types of disks in stack structures, whose probabilities are determined by f. By doing so, all continuous coordinates of neighboring disks are coarse grained into three typical Voronoi cell volumes V_α (with $\alpha = 0, 1, 2$ as the type number). The free volume of this quasiparticle is thus expressed as $W(f) = V_2 f^2 + 2V_1 f(1-f) + V_0(1-f)^2 - V_d$. We set $V_2 = V_d/0.92$ and $V_0 = V_d/0.37$, which are the experimentally obtained smallest and largest Voronoi cell volumes, representing approximately the densest and loosest possible microscopic packing states of the quasiparticle. Also, we set $V_1 = (V_0 + V_2)/2$, which is consistent with the fact that the average $V_{\rm cell}$ of type-1 disks is very close to the mean of those of type-0 and type-2 disks, as shown in Fig. 4(a). The moderate evolution of average Voronoi cell volume with Φ is neglected, which we regard as a secondary mechanism compared with the stack growth. Likewise, owing to the rough constancy of the average constraint number for disks of each type when only contacts on disk faces are included [Fig. 3(b)], we establish an empirical expression for constraint number C as a function of f for this quasiparticle: $C = C_2 f^2 + 2C_1 f(1-f) + C_0(1-f)^2 = 3f + 3$, where C_α is the typical constraint number of disks of type α. This relationship links stack structures with the mechanical stability requirement. Here, $C_2 = 6$, corresponding to the two ff contacts, each providing 3 constraints, and $C_0 = 3$, corresponding to a minimum requirement of three point contacts to constrain the two rotational and one translational d.o.f. of a disk. Similarly, $C_1 = (C_0 + C_2)/2$. These empirical values are consistent with experimental data [Fig. 3(b)].

With the above volume function, we can calculate the single-particle canonical partition function $Q = \int \Theta_W g_W e^{-W/\chi} dW$, where g_W is the density of state and Θ_W picks out mechanical stable states. It is transformed to an integration of average constraint number, $Q = \int_{C_{\rm min}}^{C_{\rm max}} g_C e^{-W/\chi} dC$, to incorporate the mechanical stability requirement directly by limiting the integration range. An additional variable transformation is performed to obtain $Q = \int_{f_{\rm min}}^{f_{\rm max}} g_C e^{-W(f)/\chi} df$, where $\partial C/\partial f$ happens to be a constant and is omitted. Here, $C_{\rm max} = 6$ and, equivalently, $f_{\rm max} = 1$, representing the densest microstate. $C_{\rm min} \approx 4.2$ ($f_{\rm min} \approx 0.4$ accordingly) corresponds to the loosest stable configuration, which depends on the friction coefficient measured to be 0.63 ± 0.05 for our disks. The density of state $g_C = h_z^{C(f)}$ according to Ref. [27], where h_z is the minimum distance between microstates in the configurational space. Note that only a subspace of the configurational space of a "jammed" granular disk packing is discrete as required by the mechanical stability, corresponding to the incomplete geometric constraints of the disks imposed by contacts on disk faces. We obtain an ensemble-averaged packing fraction $\bar{\Phi}(\chi) = Q^{-1} \int_{f_{\rm min}}^{1} [V_d/(W + V_d)] \times e^{-W/\chi + C\log h_z} df$, and $\bar{f}(\chi) = Q^{-1} \int_{f_{\rm min}}^{1} f e^{-W/\chi + C\log h_z} df$. The parameter h_z is adjusted to 0.0133 so that $\bar{\Phi}(+\infty) = \Phi_{\rm RLP}$. The resulting $\bar{\Phi}(\chi)$ and ensemble-averaged stack size $\bar{N}_s = 1/(1-\bar{f})$ agree with the experimental results satisfactorily [Figs. 4(c) and 2(b)], given the crudeness of this model. According to our model, the stack formation in this system is attributed to an equilibrium sampling of the configurational space with a low compactivity.

The remaining task is to understand why the growth of stacks diminishes the global orientational order. Intuitively, the packing structural anisotropy around a thick stack should be weaker than that of a single disk: try imaging the excluded volume between two cylinders, whose dependence on their relative orientation is strong for very short cylinders (like disks), and becomes weak if their height is close to the diameter. To analyze this effect quantitatively, we calculate a local orientational order parameter $s_{\rm disk} = \langle P_2(\cos\Delta\theta)\rangle$ averaged over all Voronoi neighbors of each disk, where $\Delta\theta$ is the included angle between the orientations of each disk and its neighbor. As shown in Fig. 5(a), the correlation

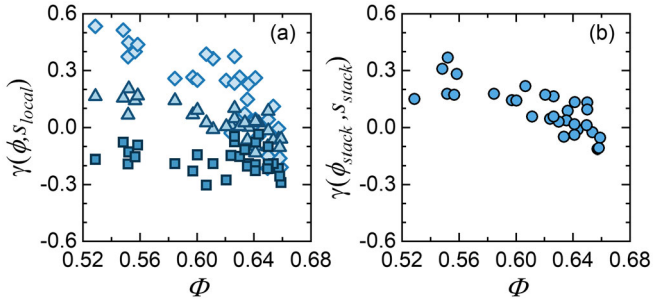

FIG. 5. (a) Correlation coefficients γ between s_{disk} and ϕ for disks of type 0 (diamonds), 1 (triangles), and 2 (squares), and (b) γ between s_{stack} and ϕ_{stack}, for packings with different Φ.

coefficient between s_{disk} and ϕ decreases as Φ increases, for disks of type 0 and 1, demonstrating clearly that the compaction effect is no longer the driving mechanism of local orientational ordering as stack grows. For disks inside stacks (i.e., type 2), the correlation coefficient is always negative due to a simple geometric reason. The flat faces of nearby disks block large free volumes of a disk, and therefore, ϕ of a disk within a stack is larger if more surrounding disks face toward the stack. Therefore, local configurations with mutually perpendicular disks are preferred when stacks are large, which are frustrated with the global nematic order. This also explains the slightly negative values of S_2 for large Φ. To reveal the connection between global orientational disordering and stack growth more straightforwardly, we calculate each stack's packing fraction ϕ_{disk} and a similar mesoscale orientational order parameter s_{stack} of the relative orientations of a central stack and its neighboring stacks. As shown in Fig. 5(c), the correlation coefficient between them demonstrates a similar trend as S_2 versus Φ, implying a direct correspondence between the global orientational order and the preferred relative orientations in locally dense configurations. We have also noticed that stacks cannot translate freely as a whole, in comparison with individual disks. These results remind us of the mutually frustrated locally favored stacks observed in colloidal hard disk systems, which hinder the evolution toward a globally ordered state [15]. A columnar phase may emerge possibly with a first-order phase transition like the one between the random and crystalline packing states of granular spheres [31].

In this Letter, we study the extraordinary structural properties of granular disk packings, and how stacks grow and diminish the global orientational order upon compaction. This unusual structural transformation can be well understood by Edwards volume ensemble theory and the packing effect of stacks, demonstrating essential differences from the thermal-equilibrium isotropic-nematic phase transition. On the other hand, it also seems that the gap between a mechanically stable granular disk packing and the liquid state of colloidal hard disks is much narrower than it appears. Both systems exhibit a phase transformation behavior associated with frustrated mesoscale stack structures inhibiting a global ordering. Therefore, the models developed here based on the equilibrium statistical mechanics of granular disk packings can shed light on the nonequilibrium states and aging phenomena of discotic liquid crystals and clay particles. In future investigations, a fine-tuning of packing preparation protocol and interparticle friction may help mapping a complete nonequilibrium phase diagram of disklike particle packings. Also, a general statistical mechanical framework linking thermal and granular systems is expected to predict the universal nonergodic characteristics in various disk assemblies.

This work is supported by the National Natural Science Foundation of China (Grant No. 11904102).

*Corresponding author: cjxia@phy.ecnu.edu.cn

[1] H. N. W. Lekkerkerker and G. J. Vroege, Phil. Trans. R. Soc. A **371**, 20120263 (2013).
[2] J. T. Lopes, F. Romano, E. Grelet, L. F. M. Franco, and A. Giacometti, J. Chem. Phys. **154**, 104902 (2021).
[3] N. Morillo, B. Martinez-Haya, and A. Cuetos, Soft Matter **17**, 8693 (2021).
[4] R. Eppenga and D. Frenkel, Mol. Phys. **52**, 1303 (1984).
[5] A. Chamoux and A. Perera, J. Chem. Phys. **108**, 8172 (1998).
[6] P. D. Duncan, M. Dennison, A. J. Masters, and M. R. Wilson, Phys. Rev. E **79**, 031702 (2009).
[7] L. Wu, H. H. Wensink, G. Jackson, and E. A. Muller, Mol. Phys. **110**, 1269 (2012).
[8] F. M. van der Kooij, K. Kassapidou, and H. N. W. Lekkerkerker, Nature (London) **406**, 868 (2000).
[9] J. A. C. Veerman and D. Frenkel, Phys. Rev. A **45**, 5632 (1992).
[10] M. Marechal, A. Cuetos, B. Martinez-Haya, and M. Dijkstra, J. Chem. Phys. **134**, 094501 (2011).
[11] H. Zewdie, Phys. Rev. E **57**, 1793 (1998).
[12] D. Caprion, L. Bellier-Castella, and J. P. Ryckaert, Phys. Rev. E **67**, 041703 (2003).
[13] M. C. D. Mourad, D. V. Byelov, A. V. Petukhov, and H. N. W. Lekkerkerker, J. Phys. Condens. Matter **20**, 494201 (2008).
[14] M. C. D. Mourad, A. A. Verhoeff, D. V. Byelov, A. V. Petukhov, and H. N. W. Lekkerkerker, J. Phys. Condens. Matter **21**, 474218 (2009).
[15] M. Marechal, A. Patti, M. Dennison, and M. Dijkstra, Phys. Rev. Lett. **108**, 206101 (2012).
[16] S. Jabbari-Farouji, G. H. Wegdam, and D. Bonn, Phys. Rev. Lett. **99**, 065701 (2007).
[17] B. Ruzicka, L. Zulian, E. Zaccarelli, R. Angelini, M. Sztucki, A. Moussaid, and G. Ruocco, Phys. Rev. Lett. **104**, 085701 (2010).
[18] B. Ruzicka and E. Zaccarelli, Soft Matter **7**, 1268 (2011).
[19] R. Angelini, E. Zaccarelli, F. A. D. Marques, M. Sztucki, A. Fluerasu, G. Ruocco, and B. Ruzicka, Nat. Commun. **5**, 4049 (2014).

[20] T. Dabat, F. Hubert, E. Paineau, P. Launois, C. Laforest, B. Grégoire, B. Dazas, E. Tertre, A. Delville, and E. Ferrage, Nat. Commun. **10**, 5456 (2019).
[21] T. Dabat, P. Porion, F. Hubert, E. Paineau, B. Dazas, B. Gregoire, E. Tertre, A. Delville, and E. Ferrage, Appl. Clay Sci. **184**, 105354 (2020).
[22] M. Tyagi, T. Gimmi, and S. V. Churakov, Adv. Water Resour. **59**, 181 (2013).
[23] A. C. Perdigon-Aller, M. Aston, and S. M. Clarke, J. Colloid Interface Sci. **290**, 155 (2005).
[24] J. D. Bernal, Nature (London) **183**, 141 (1959).
[25] C. Xia, J. Li, Y. Cao, B. Kou, X. Xiao, K. Fezzaa, T. Xiao, and Y. Wang, Nat. Commun. **6**, 8409 (2015).
[26] S. F. Edwards and R. B. S. Oakeshott, Physica (Amsterdam) **157A**, 1080 (1989).
[27] C. Song, P. Wang, and H. A. Makse, Nature (London) **453**, 629 (2008).
[28] A. Baule, R. Mari, L. Bo, L. Portal, and H. A. Makse, Nat. Commun. **4**, 2194 (2013).
[29] A. Baule and H. A. Makse, Soft Matter **10**, 4423 (2014).
[30] C. C. Mounfield and S. F. Edwards, Physica (Amsterdam) **210A**, 279 (1994).
[31] Y. Jin and H. A. Makse, Physica (Amsterdam) **389A**, 5362 (2010).
[32] Y. Ding, D. Gong, J. Yang, Z. Xu, Z. Wang, J. Li, B. Hu, and C. Xia, Soft Matter **18**, 726 (2022).
[33] S. S. Ashwin, M. Zaeifi Yamchi, and R. K. Bowles, Phys. Rev. Lett. **110**, 145701 (2013).
[34] A. Barrat, J. Kurchan, V. Loreto, and M. Sellitto, Phys. Rev. Lett. **85**, 5034 (2000).
[35] A. Baule, F. Morone, H. J. Herrmann, and H. A. Makse, Rev. Mod. Phys. **90**, 015006 (2018).
[36] L. Berthier and G. Biroli, Rev. Mod. Phys. **83**, 587 (2011).
[37] T. Dabat, A. Mazurier, F. Hubert, E. Tertre, B. Gregoire, B. Dazas, and E. Ferrage, Materials **11**, 1972 (2018).
[38] See Supplemental Material at http://link.aps.org/supplemental/10.1103/PhysRevLett.131.098202 for details regarding the experiment, image processing and contact identification methods, structural quantifications (including correlation functions and geometric constraints), and derivation of global packing volume variance.
[39] F. M. Schaller, S. C. Kapfer, M. E. Evans, M. J. F. Hoffmann, T. Aste, M. Saadatfar, K. Mecke, G. W. Delaney, and G. E. Schroder-Turk, Philos. Mag. **93**, 3993 (2013).
[40] T. Aste, M. Saadatfar, and T. J. Senden, Phys. Rev. E **71**, 061302 (2005).
[41] L. Onsager, Ann. N.Y. Acad. Sci. **51**, 627 (1949).
[42] A. Jaoshvili, A. Esakia, M. Porrati, and P. M. Chaikin, Phys. Rev. Lett. **104**, 185501 (2010).
[43] Y. Yuan *et al.*, Phys. Rev. Lett. **127**, 018002 (2021).
[44] E. R. Nowak, J. B. Knight, E. Ben-Naim, H. M. Jaeger, and S. R. Nagel, Phys. Rev. E **57**, 1971 (1998).